First-principles calculation of native defect densities in $Hg_{0.8}Cd_{0.2}Te$

M. A. Berding, M. van Schilfgaarde, and A. Sher
SRI International, Menlo Park, California 94025
(Received 3 March 1994)

We use a quasichemical formalism to make quantitative predictions of the native point defect densities in $Hg_{0.8}Cd_{0.2}Te$. The electronic contribution to the defect-formation free energy is calculated using the self-consistent first-principles full-potential linearized muffin-tin orbital method and the local-density approximation (LDA). A gradient correction is added to the LDA result so that absolute reference to the chemical potential of the mercury vapor phase can be made. A Green's function approach based on a valence force field plus a point Coulomb model is used to calculate the vibrational contributions to the defect free energy (both energy and entropy). We find the double acceptor mercury vacancy is the dominant defect, in agreement with previous interpretations of experiments. The tellurium antisite is also found to be an important defect in this material. Predictions of the low-temperature hole concentrations are made as a function of annealing temperature and compared with available experiments. The order of magnitude of our predictions agrees well with experimental results, and discrepancies can be attributed to contributions to the free energy that we have neglected or to inaccuracies in the intrinsic reaction constant used. Suggestions for further experimental work are made.

I. INTRODUCTION

The pseudobinary semiconductor alloy $Hg_{1-x}Cd_xTe$ with $x=0.22$ is currently the material of choice for high-performance detectors in the long-wavelength infrared (8–14 μm). Unlike other II-VI systems, both extrinsic p- and n-type doping can be achieved in $Hg_{0.8}Cd_{0.2}Te$, although in as-grown material the electrical properties are often determined by native point defect concentrations. The dominant defect is believed to be a double-acceptor mercury vacancy;[1] post-growth low-temperature mercury-saturated anneals are routine for the reduction of the mercury vacancy concentration. As in other semiconductors, it is more difficult to establish the presence and identity of neutral and compensating point defects, much less to determine their concentrations. Diffusion measurements[2] indicate the presence of mercury vacancies and mercury interstitials, as well as tellurium interstitials, although no unambiguous determination of their densities can be made from these experiments.

Although extended defects such as dislocations often appear to be the performance limiter in current state-of-the-art $Hg_{0.8}Cd_{0.2}Te$ devices,[3–5] a number of mysteries still persist that may relate to native point defects. (1) For operation at 40 K, there is a variation in R_0A_j and lifetime among pixels with no etch pits,[3] indicative of spatial nonuniformity in the material that is unrelated to dislocations. (2) An as yet unidentified donor limits the minimum n-type carrier concentrations obtainable during a mercury-saturated low-temperature anneal of the material. While the pressure and temperature dependence of this residual donor does not appear to correlate with the equilibrium dependences of any native point defect,[6] the nearly universal presence of the donor in liquid phase epitaxy (LPE), solid-state recrystalized, and molecular beam epitaxy (MBE) materials and its elusive nature do suggest that a native point defect is responsible. (3) Undoped LPE material that has been subjected to a low-temperature mercury-saturated anneal and nominally converted to n type shows an anomalously low mobility. One interpretation is that it is a consequence of interpenetrating p- and n-type regions, with the high effective-mass holes lowering the measured Hall mobilities.[7] If this model proves to be correct, it may well be a native point defect that causes nonuniform annealing of the material. To overcome this low mobility, a donor impurity is added in concentrations above that of the unknown residual donor. Thus, to lower the n doping to desirable levels, an understanding of the origin of the doping, and the low mobility and a recipe for its elimination are neeeded. (4) The identity of the primary Shockley-Reed-Hall (SRH) recombination centers has not been established; if they can be correlated with native point defects, strategies for their elimination can be developed. (5) MBE material is often n type as grown[8] and may be related to a nonequilibrium population of native point defects.

Unraveling the matrix of usually indirect and often contradictory experimental data on the native point defects in semiconductors is a complicated task, especially when the defects may be spatially varying. Numerous theoretical efforts have utilized first-principles methods to elucidate the properties of native point defects in the group IV, III-V, and II-VI semiconductors (see, for example, Refs. 9–12). While these studies have led to much insight into the properties of the point defects, no quantitative predictions of the defect densities were made. Several earlier theoretical studies have looked at the properties of defects in HgCdTe,[13–16] although once again no

quantitative predictions of defect densities were given.

Our goal in this paper is to theoretically identify the important native defects in HgCdTe, to calculate their densities as a function of growth and processing conditions, to substantiate the experimentally deduced properties of the native defects, and to begin to unravel the remaining mysteries in this material. To express the concentration of the native point defects in terms of their formation free energies, we employ the quasichemical formalism. In addition to the electron and hole, we have included eight native point defects (and their ionized species) in the analysis: the mercury and tellurium vacancies, the mercury and tellurium antisites, and two types of mercury and tellurium tetrahedral interstitials—one surrounded by four cation near neighbors and one surrounded by four anion near neighbors. As we will show, we have attempted to incorporate all of the important contributions to the free energy and adopt a first-principles approach for most of the quantities we calculate. The only significant empirical data we employ are those needed to obtain the temperature-dependent intrinsic reaction constant. Our calculated native defect concentrations are in quantitative agreement with the available experiment data. Preliminary results of this work have been published previously.[17]

A number of features make our study of defects in $Hg_{0.8}Cd_{0.2}Te$ unique and permit us to calculate absolute defect concentrations.

(i) To calculate the electronic contribution to the defect formation free energies we employ the self-consistent first-principles full-potential (FP) linearized muffin-tin orbital (LMTO) method[18] and the local-density approximation (LDA). The LMTO method is well suited for compounds containing d electrons, such as $Hg_{1-x}Cd_xTe$.

(ii) Because the LDA overbinds, we have also employed gradient corrections to the LDA of the Langreth-Mehl-Hu type.[19] These corrections greatly improve the overbinding found in the LDA.[20] We believe the calculated energies are precise enough that we may make comparison with atoms referenced to the free atom, and therefore by combining these energies with the translational energy of the atoms in the vapor phase, we are able to calculate the chemical potential for a monoatomic mercury vapor.

(iii) A Green's function formalism within a valence force model plus point-charge ionic model is used to calculate the vibrational contribution to the defect-formation free energy, both the enthalpy and entropy.

(iv) The combination of the electronic, translational, and vibrational free energies calculated in (i)–(iii) encompass the primary contributions to the total defect-formation free energies when referenced to a mercury vapor. The total defect-formation free energy is then incorporated into a quasichemical formalism,[21] and predictions of absolute defect concentrations as a function of the thermodynamic variables temperature and pressure can be made.

The remainder of the paper is organized as follows. In Sec. II we describe the quasichemical formalism used to calculate the neutral native defect concentrations and its extension for ionized defects and alloys. The calculations of the defect-formation free energies are discussed in Secs. III and IV for the electronic and vibrational contributions, respectively. In Sec. V we present the results of our calculations and a comparison with available experimental results. We end with a brief summary and conclusions of our work in Sec. VI.

II. DEFECT CONCENTRATIONS

A. Quasichemical formalism in compounds

We begin by outlining the formalism employed to calculate the defect concentrations in a compound as a function of external parameters. In Sec. II C we discuss extensions of the formalism necessary to treat the low-x alloy $Hg_{1-x}Cd_xTe$.

The defect reactions for the compound AC to be considered in this paper are listed in Table I. We have chosen the AC unit cell and A in the phase R as our reference states for the calculation of the reactions' free energies. From Gibbs's phase rule we know that for a system of two components (A and C) and two phases (one of which is the AC zinc blende solid) there are two degrees of freedom. For this paper we shall assume that temperature is one degree and that the chemical potential of an external reservoir of A or C atoms is the other. The chemical potential is chosen to be consistent with the experimental situation to be modeled. We shall choose our reference state to be the mercury vapor and therefore choose to reference our reaction energies to the AC solid and A_R, which will be taken as the monoatomic mercury vapor (extensions of this analysis to the alloys are discussed in Sec. V).

Reference to other reservoirs can be obtained by con-

TABLE I. Defect reactions considered for compound AC. The notation is as follows: The primary symbol refers to the species, the subscript refers to the site that the species occupies, with no subscript indicating that the species is occupying its usual lattice site. V corresponds to a vacancy, I an interstitial, R some external reference state, and X a generic defect. Two types of interstitials are considered, both occupying tetrahedral sites, the first surrounded by four cation nearest neighbors I_C, the second surrounded by four anion nearest neighbors I_A. Following the notation of Kröger (Ref. 21), an $\times$ superscript corresponds to a neutral species, a prime to a negatively charged species, a bullet to a positively charged species, and e' and $h^\bullet$ are an electron and a hole, respectively.

AC	$\longrightarrow$	$V_A^\times C + A_R$	(1)
A_R	$\longrightarrow$	$AV_C^\times$	(2)
$2A_R$	$\longrightarrow$	$AA_C^\times$	(3)
$2AC$	$\longrightarrow$	$C_A^\times C + 2A_R$	(4)
A_R	$\longrightarrow$	$A_{I_A}^\times$	(5)
A_R	$\longrightarrow$	$A_{I_C}^\times$	(5′)
AC	$\longrightarrow$	$C_{I_A}^\times + A_R$	(6)
AC	$\longrightarrow$	$C_{I_C}^\times + A_R$	(6′)
$X^\times$	$\longrightarrow$	$X^{z\prime} + zh^\bullet$	(7)
$X^\times$	$\longrightarrow$	$X^{z\bullet} + ze'$	(8)
$e' + h^\bullet$	$\longrightarrow$	0	(9)

sidering the additional reaction

$$AC \rightarrow A_R + C_R \tag{1a}$$

or for molecular species as the reference

$$AC \rightarrow \frac{1}{n_A} A_{n_A} + \frac{1}{n_C} C_{n_C} , \tag{1b}$$

where n_i is the appropriate integer, and by taking linear combinations of these with the reactions in Table I.

We are not restricted to specifying the temperature and a chemical potential of one of the species as the two degrees of freedom, but could choose instead another particular set, including, for example, the stoichiometry of the system.[10] While other choices are possible, usually one does not know *a priori* the material's stoichiometry.

Assuming that the defect densities are small and that they are noninteracting, from the law of mass action we can write the reaction constant for each of the neutral defect reactions in Table I as[21,22]

$$K_{X^\times} \equiv \theta \exp\left(-\frac{F_{X^\times}}{k_B T}\right) = [X^\times] , \tag{2}$$

where $[X^\times]$ is the density of the neutral defect X, θ is the number of unit cells per volume and converts $[X^\times]$ from site fraction to defects per unit volume, and $F_{X^\times}$ is the free energy for the neutral defect reaction. The free energy for any defect X can be written as the sum

$$F_X = F_X^{\text{vib}} + F_X^{\text{elect}} + F_X^{\text{trans}} + k_B T \ln(G), \tag{3}$$

where k_B is Boltzmann's constant, and F_X^{vib} is the vibrational, F_X^{elect} is the electronic, and F_X^{trans} is the translational energy contribution to the reaction free energy, and G accounts for the degeneracies of the reactants. In the quasichemical approximation, $G = (g_C g_D)/(g_A g_B)$ for the reaction $A + B \rightarrow C + D$, where g_i is the degeneracy of reactant i. Once $F_{X^\times}$ is know for a given reaction, $K_{X^\times}$ can be evaluated and the defect concentration can be determined. The difficulty, of course, is in the evaluation of $F_{X^\times}$, which is discussed in Secs. III and IV.

B. Ionized defects and the intrinsic reaction constant

The above discussion applies to the neutral defect densities. In most semiconductors the native point defect will have one or more localized levels in the band gap, allowing for multiple ionization states of the defect. We thus need to calculate the concentration of these ionized defects, in addition to the neutral concentrations discussed above, to obtain the total defect populations. Once the energies of the localized levels are determined (Sec. III E) their populations can be calculated via

$$\frac{[X']}{[X^\times]} = \frac{g_{X'}}{g_{X^\times}} \exp\left(\frac{\mu_F - E_a - F_{X'}^{\text{vib}} + F_X^{\text{vib}}}{k_B T}\right) \tag{4}$$

for an acceptor and

$$\frac{[X^\bullet]}{[X^\times]} = \frac{g_{X^\bullet}}{g_{X^\times}} \exp\left(\frac{E_d - \mu_F - F_{X^\bullet}^{\text{vib}} + F_X^{\text{vib}}}{k_B T}\right) \tag{5}$$

for a donor state of the defect X. A bullet superscript indicates a positive charge and a prime a negative charge, E_a and E_d are the acceptor and donor one-electron ionization energies with respect to the valence and conduction band (both defined as positive for states in the gap), and μ_F is the Fermi energy. Although the last term in the exponential, $-F_{X^{z'}}^{\text{vib}} + F_{X^\times}^{\text{vib}}$, should rightly be there, and corresponds to the difference in the vibrational free energy of the neutral and ionized defect, it has never been considered previously and for the present we shall neglect it too.

For multiply ionized defects with positive Hubbard U's [reactions (7) and (8) in Table I], the above expression for the number of ionized acceptors generalizes to

$$\frac{[X^{z'}]}{[X^\times]} = \frac{g_{X^{z'}}}{g_{X^\times}} \exp\left(z\mu_F - E_a^1 - \cdots - E_a^z - F_{X^{z'}}^{\text{vib}} + F_{X^\times}^{\text{vib}}\right) , \tag{6}$$

where z is an integer and E_a^i is the ionization energy of the ith ionization level. A similar generalization applies for the donor levels.

For each ionized defect concentration, we introduced one equation. In addition, though, we have two new unknowns, the Fermi energy and either the electron or hole concentration. Thus two additional equations are needed.

First, we have the additional reaction for the generation of electron-hole pairs across the band gap, reaction (9) in Table I, and the corresponding intrinsic reaction constant

$$K_{pn} = [h^\bullet][e'] = pn , \tag{7}$$

where $p \equiv [h^\bullet]$ and $n \equiv [e']$. In general, K_{pn} depends on the shapes of the conduction and valence bands, the band gap energy, the Fermi energy (for degenerate statistics), and the temperature variation of these quantities. Several limits are often encountered in the evaluation of K_{pn}. First, when the conduction and valence bands are parabolic, although not necessarily isotropic, $E \propto k^2$, and the reaction constant can be written in terms of the Fermi-Dirac integrals as

$$K_{pn} = 4\left(\frac{2\pi k_B T}{h^2}\right)^3 (m_h m_e)^{3/2} \times \mathcal{F}_{1/2}\left(\frac{\mu_F - E_c}{k_B T}\right) \mathcal{F}_{1/2}\left(\frac{E_v - \mu_F}{k_B T}\right) , \tag{8}$$

where $\mathcal{F}_{1/2}$ is the Fermi-Dirac function; E_c, E_v, and μ_F are the conduction band, valence band, and Fermi energies, respectively; m_h and m_e are the hole and electron density-of-states effective masses, respectively; and h is Planck's constant. In the nondegenerate limit, this reduces to the familiar expression

$$K_{pn} = 4\left(\frac{2\pi k_B T}{h^2}\right)^3 (m_h m_e)^{3/2} \exp\left(\frac{E_v - E_c}{k_B T}\right) , \tag{9}$$

which is independent of the Fermi energy. For the general case, which will apply even at moderate temperatures for narrow-gap HgCdTe, K_{pn} depends on the extrinsic carrier densities through its dependence on μ_F. Moreover, the conduction band in this narrow-gap material is not well represented by a parabola, but is rather more hyperbolic.[23] Because the hyperbolic dispersion relation approaches a linear dependence away from the band edge, we will for the present assume a linear dispersion relationship of the form $E = \alpha k$. In this case the intrinsic reaction constant becomes

$$K_{pn} = 2\left(\frac{2\pi k_B T m_h}{h^2}\right)^{3/2} \frac{2}{\pi^2}\left(\frac{k_B T}{\alpha}\right)^3 \times \mathcal{F}_2\left(\frac{\mu_F - E_c}{k_B T}\right)\mathcal{F}_{1/2}\left(\frac{E_v - \mu_F}{k_B T}\right), \quad (10)$$

where $\mathcal{F}_2$ is the Fermi-Dirac integral of order 2.

The requirement of charge neutrality leads to a second additional equation:

$$\sum_i \sum_z z[X_i^{z\prime}] + [e'] = \sum_i \sum_z z[X_i^{z\bullet}] + [h^\bullet], \quad (11)$$

where i sums over the various defects and z sums over the various ionization states of the defect X_i.

C. Quasichemical formalism in alloys

We wish to generalize the above formalism to the ideal cation substituted pseudobinary alloy $A_{1-x}B_xC$. It is perhaps easiest to demonstrate the generalization with a specific defect reaction, for example, a neutral vacancy on the cation sublattice. In the compound AC the formation reaction is given by reaction (1), Table I:

$$AC \rightarrow V_\alpha^\times C + A_R, \quad (12)$$

where V_α indicates a vacancy on the cation sublattice. In the alloy a neutral vacancy on the α sublattice can form via the same reaction. The only difference comes in the evaluation of the reaction constant. In the compound the vacancy density is given by

$$[V_\alpha^\times] = \theta \exp\left(\frac{-F_{V_\alpha^\times}}{k_B T}\right) \quad (13)$$

and in the alloy it is given by

$$[V_\alpha^\times] = \theta(1-x)\exp\left(\frac{-F'_{V_\alpha^\times}}{k_B T}\right), \quad (14)$$

where $-F'_{V_\alpha^\times}$ is the reaction free energy corresponding to Eq. (12) in the alloy. The factor of $(1-x)$ results from the configurational entropy contribution to the chemical potential of A on a lattice site (ls), $k_B T \ln([A_{ls}]/[ls]) \simeq k_B T \ln(x)$. Because we have assumed that the defect concentrations are small, the configurational entropy contribution to the chemical potential of A in the compound AC is $k_B T \ln([A_{ls}]/[ls]) \simeq 0$. In both the compound and the alloy θ is the same.

In addition to Eq. (12), in the alloy the vacancy on the α sublattice can also form via the reaction

$$BC \rightarrow V_\alpha^\times C + B_R \quad (15)$$

with

$$[V_\alpha^\times] = \theta(x)\exp\left(\frac{-F''_{V_\alpha^\times}}{k_B T}\right), \quad (16)$$

where $F''_{V_\alpha^\times}$ is the reaction free energy corresponding to Eq. (15) in the alloy. Now the vacancy concentrations predicted by Eqs. (14) and (16) must be equal and thus

$$(1-x)\exp\left(\frac{-F'_{V_\alpha^\times}}{k_B T}\right) = (x)\exp\left(\frac{-F''_{V_\alpha^\times}}{k_B T}\right). \quad (17)$$

It is apparent that this simply corresponds to the difference of Eqs. (12) and (15)

$$A_R + BC \rightarrow AC + B_R, \quad (18)$$

that is, the exchange of an A and B on a lattice site, which is a reaction in the alloy in equilibrium with A_R and B_R. An analysis similar to the above applies for the anion antisite C_α, which also substitutes on the cation sublattice.

In the pseudobinary alloy, the vacancy free energies $F_{V_\alpha^\times}$ and $F'_{V_\alpha^\times}$ appearing in Eqs. (13) and (14) may be different. The energy of a vacancy depends on the local configuration of the surrounding lattice; this changes in the second and more distant neighbor shells for the cation vacancy and the anion antisite in the cation substituted alloys. A completely rigorous approach would treat each kind of vacancy uniquely; indeed in a previous work[15] we found a configuration dependence of the vacancy in the $A_{0.5}B_{0.5}C$ lattice of several tenths of an eV, varying approximately linearly in the number of A atoms in the second neighbor shell. Here we have ignored this refinement and assumed the A vacancy and C antisite surroundings are totally of species A. This is justified to some extent because we are interested in low x compositions of $Hg_{1-x}Cd_xTe$.

For defects on the C sublattice (e.g., the anion vacancy and the cation antisites) as well as interstitial atoms in certain tetrahedral sites, one must more carefully consider the complications from the alloy because disorder is found already for nearest neighbors. For systems in which these classes of defects are important, the configuration dependence of the surrounding sublattice must be taken into account. For low x $Hg_{1-x}Cd_xTe$ we find the densities of these defects to be quite low and thus the error incurred in using the electronic energies calculated for the pure AC compound will not impact the major conclusions of our work.

Finally, the band gap is one other important consideration when comparing the alloy to the pure compound. This is of particular importance for the intrinsic reaction constant and we employed an empirical fit to the temperature dependence of the alloy band gap and intrinsic

carrier concentration that are used to calculate K_{pn}. This is presented in detail in Sec. III G.

III. CALCULATION OF DEFECT FORMATION FREE ENERGY: ELECTRONIC CONTRIBUTION

A. Full-potential LMTO calculations

Total energy calculations for the defect reactions were all obtained with a full-potential version[24] of the LMTO method in the local-density functional approximation of von Barth and Hedin.[25] This method has been tested extensively for most of the elemental *sp* and *d* bonded solids, the II-VI, III-V, and column IV semiconductors, and a host of other solids. Our results, which will be reported elsewhere,[20] show good agreement with experiments for all systems studied, with small and systematic errors in structural and mechanical properties. The most prominent error, particularly for the present purposes, is the overbinding of the solid.

In the FP LMTO method, the only important approximation we make beyond the local-density approximation lies in the treatment of the interstitial matrix elements. The LMTO method employs an atom-centered basis, represented by Hankel functions in the interstitial. For the calculations presented here, the basis consisted of a "triple kappa" basis 22 orbitals per atom, with energies -0.01, -1, and -2.3 Ry for the s and p orbitals and -0.01 and -1 Ry for the d orbital. Inside the muffin-tin (MT) spheres, wave functions are represented by spherical harmonics and numerically tabulated radial functions. The electron density and potential can be similarly represented since the density generated by a Hamiltonian is obtained by summing over the eigenvectors. Outside the MT spheres, another treatment is necessary. Methfessel[26] developed a simple, efficient way to represent the density and potential in the interstitial by extrapolation from the edges of MT spheres, where the value is well known. The electron density is represented in the interstitial as a linear combination of Hankel functions that are chosen to match the value and slope of the function at each MT sphere. Two Hankels per site and lm are enough to match the values and slopes at all MT spheres. This representation of the density throughout the interstitial is approximate, although it becomes exact near any MT sphere. Extensive tests show that the approximation works very well for close-packed systems, but the errors can become significant when the packing is poor. To ensure a good fit to the charge density and potential in the interstitial region of the zinc blende solids, we include empty spheres at each tetrahedral interstitial site (rendering the sphere packing bcc for the ideal lattice). In addition, we added orbitals to the basis by centering them on the empty spheres. The addition of $2s$ and $2p$ orbitals changed the energy by approximately 0.1 mRy/atom, showing that the basis is nearly complete.

To assess the validity of the interstitial approximation for the representation of the charge density and interstitial matrix elements, an alternative approach was developed,[24] which is similar to a procedure described by Jones and Sayyesh.[27] When calculated in this way the total energies changed by approximately 1 mRy/atom, showing that the approximation is a good one.

Both the charge density inside the spheres and the tails of Hankel functions centered on a neighboring sphere were expanded to $l = 6$. We estimate that the error introduced by truncation at $l = 6$ to be about 1 mRy/atom, in line with other errors in the method. The core was allowed to relax during the self-consistency cycle. The semicore d electrons in the tellurium were treated explicitly as valence states in a second panel; explicit treatment of these states was found to introduce a small but significant correction to the total energy. For the 16-atom cells, the Brillouin zone integrals were done by a sampling method for the charge density and the linear tetrahedron method for the band–structure energy, augmented by Blöchl weights, and a mesh of four divisions was used (six k points). Checks showed that this was sufficient to converge the energy to 1 mRy/cell.

B. Supercell approximation

Supercells are used in which a periodic array of defects is constructed. Defect formation energies are calculated from a difference in total energies of the compound with and without the defect. For example, if we denote $\mathcal{E}_j(V_A)$ as the energy of a supercell containing j lattice sites and one A vacancy, the energy for defect reaction (1) in Table I is given by

$$E(V_A) = \mathcal{E}_j(V_A) + E(A_R) - \mathcal{E}_j(AB) \ , \tag{19}$$

where $E(A_R)$ is the energy of an A atom in the reference state R and $\mathcal{E}_j(AB) = jE(AB)$, where E_{AB} is the energy of an ideal AB unit cell. For some defects the number of lattice sites changes in the reaction; for example, for the formation of the B antisite via reaction 4 in Table I, the formation energy is given by

$$E(B_A) = \mathcal{E}_j(B_A) + 2E(A_R) - \mathcal{E}_{j+2}(AB). \tag{20}$$

Because we wish to calculate the formation energies in the dilute limit, we use the largest supercell computationally feasible. For this paper, all calculations were done using 16-atom supercells.

C. Gradient corrections to the local density

The local-density approximation generally overbinds the solids. Several systematic extensions of the local-density function have been proposed that are based on generalized gradient approximation for the exchange and correlation energies. We have considered one of these extensions, that proposed by Langreth and Mehl,[19] and have examined the systematics in the gradient corrections to the lattice constants, cohesive energies, bulk modulus, and other elastic constants for a wide array of solids;[20] preliminary results of that work for the zinc blende semiconductors are shown in Table II. With few exceptions,

TABLE II. Bulk cohesive energies with and without the gradient corrections (GC) to the local density (LD), and comparison with experiment.

	Cohesive energy (eV/bond)		
Compound	LD	GC	Experiment
Si	2.58	2.31	2.32
Ge	2.22	1.88	1.94
AlP	2.35	2.05	2.13
AlAs	2.17	1.85	1.89
AlSb	1.91	1.61	1.76
GaP	2.08	1.76	1.78
GaAs	1.91	1.56	1.63
GaSb	1.70	1.36	1.48
InP	1.89	1.56	1.74
InAs	1.77	1.42	1.55
InSb	1.60	1.26	1.40
ZnS	1.82	1.53	1.59
ZnSe	1.64	1.35	1.29
ZnTe	1.43	1.15	1.20
CdTe	1.33	1.04	1.10
HgS	1.29	0.94	1.02
HgSe	1.19	0.84	0.85
HgTe	1.09	0.76	0.81

the gradient correction systematically improves the prediction of the cohesive energy, although the prediction of the elastic constants often worsens slightly. The improvement in the cohesive energy is largely due to improvement in the calculation of the total energy of the free atoms, rather than the solid.

Here we are interested in calculating total energies for reactions in which a constituent is exchanged between the solid and the vapor, and thus the errors inherent in the local-density calculation of the cohesive energy will be present in these energies also. Because the relaxations do not change significantly when gradient corrections are added, we have completed the majority of the calculation, including the relaxation, within the FP LMTO. The gradient correction energy, calculated at the LDA-determined relaxed positions, is then added to the LDA energy.

D. Relaxation

In general the lattice relaxes in the presence of a defect, thereby lowering the lattice energy. In the dilute defect limit, the radial relaxation of the lattice extends to infinity.[28] In the supercells we account for this relaxation by allowing the overall lattice constant of the supercell to relax to minimize the supercell total energy. Because HgTe and CdTe are nearly lattice matched and their elastic constants are the same, the defect relaxations in pure HgTe should be comparable to those in the HgCdTe alloys. Second, for the most important defects, we permit the radial relaxation of the defect near-neighbor atoms. For the on-site defects (the vacancies and antisites) we permit only the nearest-neighbor atoms to relax. Estimates of these relaxation energies are given in Sec. V.

Relaxation energies are calculated only for the neutral defects and are assumed comparable in the ionized defects. Nonradial relaxations such as the trigonal and tetragonal distortions that split the degeneracy of the triply degenerate T_2 states may be important and may differ substantially for the different charge states of the system. Because the symmetry of the distortion depends on the charge state of the defect, distortions and charge states must be treated simultaneously. These distortions have not been considered in this paper.

E. Localized defect levels

The calculation of the ionization states of the defects is perhaps the most difficult part of the calculation of the native defect concentrations, in a large part because of the inadequacies of the LDA in predicting the band gap of the semiconductors. This is additionally complicated by the fact that our calculations were done for HgTe, which is known experimentally to be a semimetal with a negative band gap of -0.3 eV, so that even if the LDA band gap were correct, we would still have a zero-gap material. Furthermore, because the Coulomb fields associated with a defect may be extended, we expect that very large supercells will be needed to isolate the localized levels of an individual defect.

We have developed a method to calculate the location of localized defect levels in the band gap and have applied it to the arsenic antisite defect in GaAs. This defect was chosen because of its technological importance and because these levels have been determined experimentally by Weber *et al.*[29] Calculations were done within the atomic-spheres approximation so that we could examine the convergence of our results going to large (128-atom) supercells. Our approach is similar to that discussed by Van de Walle *et al.*[30] in which the shift in the Fermi level is examined as electrons are added to (or removed from) the defect, with a compensating uniform background charge added so as to maintain charge neutrality. We find good agreement with experiments of the two antisite donor levels. We also have found these energies agreed closely with the positions of peaks in the density of states, when referenced to the top of the valence band. Details of the calculation will been given elsewhere.

Because the compositions of HgCdTe of interest here have narrow band gaps, the determination of the exact location of the defect levels in the band gap is not as important for the purpose of calculating the defect concentrations as in a wider-gap semiconductor such as GaAs, although the identification of the position of defect levels is useful in understanding mechanisms limiting carrier lifetimes. We have used the 54-atom supercells of HgTe to determine the type (acceptor or donor) of the various native defects based on the position of the Fermi level with respect to the states that lie within ~ 0.1 eV above

the valence band edge. In addition, an assessment of whether the state is a single or double donor or acceptor and whether the state is shallow or deep has been made based on the position of the density of states peaks. For the mercury vacancy, we follow the arguments of Cooper and Harrison[31] and assume that it is a negative-U center, with the neutral and double acceptor states being the only observable states; this assumption is consistent with the observation that the mercury vacancies are always found to be doubly ionized acceptors.[1]

F. Ionization state degeneracy

The degeneracy of the various ionization states of each defect may differ and must be determined[32] to complete the calculation of the density of ionized defects. As an example, we consider the A vacancy in a II-VI material and use tight-binding language for the purpose of discussing the defect states. There are four dangling anion hybrids, each donating 1.5 electrons to the system, for a total of six electrons at the vacancy site. Although we have not explicitly calculated it, for the purpose of computing state degeneracy, we assume that a symmetry lowering Jahn-Teller distortion will take place whenever there is a state degeneracy beyond two (for spin) and a partial occupancy of that state. Thus we assume that the highest filled vacancy level in the neutral state is doubly occupied with one electron spin up and one spin down, and that the level can accept no other electron. Because there is only one unique configuration for this state, the state has a degeneracy of one. For the single acceptor state in which one electron has been added to the vacancy, the extra electron can either go in spin up or spin down, with equivalent energies. The degeneracy of the state is therefore two. Finally, if the vacancy is a doubly ionized acceptor, the lowest energy configuration for the two additional electrons is with one spin up and one spin down, with a net state degeneracy of one. This assignment of degeneracies—one, two, and one for the neutral, singly ionized, and doubly ionized acceptor, respectively—will hold even if the state is a Hubbard negative-U state, although in this case, the singly ionized state will not be occupied.

A similar argument follows for the other donor and acceptor defect levels. In general, for the II-VI materials we find a degeneracy of one for the neutral defect state, two for the singly ionized state, and one for the doubly ionized state.

G. Intrinsic reaction constant

We are interested in calculating native point defect densities at the relatively high temperatures at which equilibration occurs. It is difficult to calculate K_{pn} theoretically because of the difficulty in calculating the finite-temperature band structure; in general the band gap and the conduction and valence band shapes are all temperature dependent. An additional complexity in calculating K_{pn} in low x $Hg_{1-x}Cd_xTe$ is the nonparabolicity of the conduction and light-hole bands near their extrema.[23]

For the purposes of evaluating the defect concentrations, we have calculated K_{pn} using Eq. (10) with $m_h^* = 0.443$;[33] an empirical relationship for the dependency of the band gap on composition x and temperature[34]

$$\begin{aligned} E_g(x,T) &= E_c - E_v \\ &= -0.302 + 1.93x - 0.810x^2 + 0.832x^3 \\ &\quad +5.35\times 10^{-4}T(1-2x), \end{aligned} \tag{21}$$

which was fit for $4.2 \le T \le 300$ K; and a linear dispersion relationship for the conduction band with α chosen to yield good agreement with experimental values of the intrinsic carrier concentrations[33] for $T < 400$ K. We assume that the intrinsic reaction constant thus computed is valid at temperatures up to 655 °C, although there have been no measurements above ~400 K to substantiate this extrapolation.[35]

IV. CALCULATION OF DEFECT-FORMATION FREE ENERGY: VIBRATIONAL CONTRIBUTION

When a defect is introduced into the lattice, the vibrational modes of the system are modified. We must include in our calculation of the defect formation free energy a term that comes from modifications of the vibrational spectrum. Most authors neglect this contribution to the formation free energy. As we will see in Sec. V, although the electronic contribution to the free energy is dominant, the vibrational changes can be significant and they make a substantial impact on the calculated magnitude of the defect concentrations.

Although ideally the vibrational contribution to the formation energy should be calculated within LDA on the same footing as the static electronic contribution, including all of the anharmonic terms, this is a difficult and computationally demanding task. Instead, we take an alternative approach and calculate the vibrational spectrum of the zinc blende lattice using Keating's valence force-field model for the short-range elastic interactions.[36] Although experimental elastic constants were used, LDA theory actually predicts the elastic constants within 10% for HgTe and CdTe, so we could equally well have used the calculated values. Because we are dealing with an ionic crystal, we have included a point-charge model to account for the Coulombic interactions.[37] Unlike the valence force-field contributions to the dynamical matrix, the Coulomb contributions are long range in nature and induce a macroscopic electromagnetic field, which results in a screening of the transverse optical phonons. The ionic charge is chosen to yield agreement with experiments for the zone center splitting of the transverse and longitudinal optical phonons. A Green's function approach is used to evaluate the lattice-defect-induced modifications to the phonon spectrum; from the perturbed phonon density of states the change in the vibrational free energy can be calculated. Like the electronic energies, the calculations were done for pure HgTe and are assumed applicable to

TABLE III. Neutral native defect formation energies for HgTe corresponding to reactions in Table I, where A is mercury, B is tellurium, and the free atom is used as the reference state A_R. Local-density (LD) calculations were done using a 16-atom supercell, unless otherwise noted. Gradient correction (GC) energies are discussed in the text. The most important ionization states of the native point defects are also given.

Defect	Energy (eV)				Ionization state
	LD	Relaxation	GC	Total	
V_{Hg}	2.83	−0.05	−0.69	2.09	double acceptor[a]
V_{Te}	0.99	−0.01	0.49	1.47	shallow donor
Hg_{Te}	−1.00	0	1.46	0.46	deep acceptor
Te_{Hg}	4.85	−0.19	−1.54	3.12	shallow donor
$Hg_{I_{Hg}}$	0.75	−0.24	0.70	1.21	shallow donor
$Hg_{I_{Te}}$	0.81	−0.31	0.62	1.12	shallow donor
$Te_{I_{Hg}}$	4.78	−0.57	−0.83	3.38	shallow donor
$Te_{I_{Te}}$	5.17	−0.84	−0.96	3.37	shallow donor

[a]Assumed to be a negative-U center.

defect calculations in $Hg_{0.8}Cd_{0.2}Te$. We expect that this is a reasonable assumption because the elastic constants for HgTe and CdTe are nearly identical. In this paper we only consider the vibrational free energy of the neutral defects and assume

$$F^{\text{vib}}_{X^{z\prime}} \simeq F^{\text{vib}}_{X^{z\bullet}} \simeq F^{\text{vib}}_{X^{\times}} \tag{22}$$

for all ionization states. Details of the calculations are given in the Appendix. Preliminary results of this model were given previously.[14,17]

V. RESULTS AND DISCUSSION

A. Formation free energies in HgTe

Calculated defect-formation electronic energies in HgTe for the defect reactions listed in Table I and with A_R as the free mercury atom are listed in Table III. For all defects, the gradient correction for the 16-atom supercell is calculated for the relaxed configuration, as determined by the LDA calculation.

Although the total electronic formation energies listed in Table III are important contributions to the formation free energy, these energies alone cannot be used to assess the relative importance of the various defects in the solid. This is mostly due to the free energy of the atom in the reference state (in excess of its free atom electronic energy) that is not included in these electronic energies, and which is discussed in the Sec.V B. This point should be obvious because we could have just as well defined our defect reactions with respect to the tellurium molecule in the vapor phase and the HgTe solid and obtained the corresponding reaction energies that would be quite different from those in Table III.

The calculated phonon dispersion curve for HgTe is given in Fig. 1 and is in fair agreement with the experimental results. The discrepancies with the experimental curves, in particular near the Brillouin zone boundary, can be attributed for the most part to our neglect of long-range elastic interactions in the near-neighbor valence force-field model.[38] The vibrational entropy and energy contribution to the defect formation free energy are calculated from the density of phonon states; results at 500 °C are given in Table IV. Equation (A20) can be used to estimate the values at other (high) temperatures.

B. Defect reaction constants in $Hg_{0.8}Cd_{0.2}Te$

The reaction constants for each of the defect reactions listed in Table I are calculated as a function of temperature, where the reference state was taken as the monoatomic mercury vapor at pressure P_{Hg}. Electronic energies for the neutral defect formation energies are taken from Table III. Vibrational free energies are calculated using the general temperature expression, as discussed in the Appendix, although for the purpose of obtaining an analytical expression for the reaction constants with the primary temperature dependency explicitly displayed, we have fit our results for 500 °C to the high-temperature expression, Eq. (A20).

A third contribution to the formation free energy comes from the free energy of the mercury in the reference state, less the electronic energy of the free mercury atom that is contained in the electronic defect formation

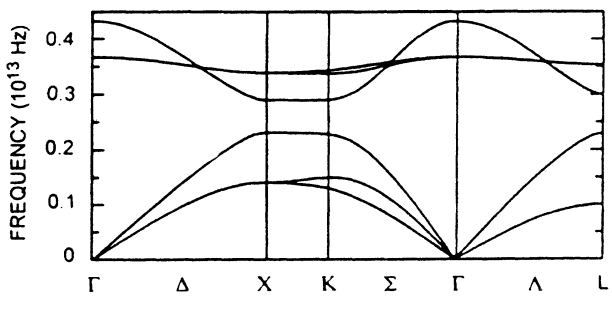

FIG. 1. Calculated phonon dispersion curve for HgTe.

TABLE IV. Entropy ($S^{\rm vib}$) and energy ($U^{\rm vib}$) contributions to the vibrational free energy in HgTe at 500 °C, for the defect reactions listed in Table I.

Defect	$S^{\rm vib}(k_B)$	$U^{\rm vib}$(eV)
$V_{\rm Hg}$	−8.9	−0.20
$V_{\rm Te}$	9.7	0.19
$\rm Hg_{Te}$	18.7	0.39
$\rm Te_{Hg}$	−18.7	−0.39
$\rm Hg_I$	9.5	0.20
$\rm Te_I$	−9.5	0.20

energies. For the vapor, we must include the translation free energy of the atoms. The chemical potential for monoatomic mercury in the gas phase is given by the standard expression from statistical mechanics

$$\mu_{\rm Hg} = kT \ln\left[\frac{P_{\rm Hg}}{kT}\left(\frac{h^2}{2\pi m_{\rm Hg} kT}\right)^{3/2}\right] . \quad (23)$$

Combining these three contributions to the reaction free energy we obtain the reaction constants for each of the defect reactions. For example, for the neutral mercury vacancy in HgTe, we obtain

$$K_{V_{\rm Hg}} = [V^{\times}_{\rm Hg}] = \theta(1-x)\frac{kT}{P_{\rm Hg}}\left(\frac{2\pi m_{\rm Hg} kT}{h^2}\right)^{3/2} \times (1.27\times 10^6 T^{-3})\exp\left(\frac{-2.09\,{\rm eV}}{kT}\right) , \quad (24)$$

where we have taken $g_{V^{\times}_{\rm Hg}} = 1$, $-F^{\rm elect}_{V_{\rm Hg}} = -2.09$, $\theta = 1.48\times 10^{22}$ cm^{-3}, and replaced $\exp(-F^{\rm vib}/k_BT)$ by $\exp[-(-0.2\ {\rm eV}+8.9k_BT)/k_BT]|_{500\,^\circ{\rm C}} \simeq 1.27\times 10^6\ T^{-3}$. Reaction constants for the eight native point defects considered in this paper are listed in Table V.

TABLE V. Reaction constants for neutral defects in $\rm Hg_{0.8}Cd_{0.2}Te$, corresponding to the defect reactions in Table I. The vibrational contribution is calculated at 500 °C and fit to the high-temperature power-law dependence [Eq. (A19)] so as to show the explicit temperature dependence. All calculations in the paper were done using reaction constants with the more exact expression for the vibrational free energies.

Defect	Reaction constant
$V^{\times}_{\rm Hg}$	$K_{V^{\times}_{\rm Hg}} = [V^{\times}_{\rm Hg}] = 1.14\times 10^{30} T^{-\frac{1}{2}} P^{-1}_{\rm Hg}\exp(\frac{-2.09}{k_BT})$
$V^{\times}_{\rm Te}$	$K_{V^{\times}_{\rm Te}} = [V^{\times}_{\rm Te}] = 4.55\times 10^{14} T^{\frac{1}{2}} P_{\rm Hg}\exp(-\frac{1.47}{k_BT})$
$\rm Hg^{\times}_{Te}$	$K_{\rm Hg^{\times}_{Te}} = [\rm Hg^{\times}_{Te}] = 4.47\times 10^{6} T^{1} P^{2}_{\rm Hg}\exp(-\frac{0.46}{k_BT})$
$\rm Te^{\times}_{Hg}$	$K_{\rm Te^{\times}_{Hg}} = [\rm Te^{\times}_{Hg}] = 3.80\times 10^{37} T^{-1} P^{-2}_{\rm Hg}\exp(-\frac{3.12}{k_BT})$
$\rm Hg^{\times}_{I_{Hg}}$	$K_{\rm Hg^{\times}_{I_{Hg}}} = [\rm Hg^{\times}_{I_{Hg}}] = 3.03\times 10^{14} T^{\frac{1}{2}} P_{\rm Hg}\exp(-\frac{1.21}{k_BT})$
$\rm Hg^{\times}_{I_{Te}}$	$K_{\rm Hg^{\times}_{I_{Te}}} = [\rm Hg^{\times}_{I_{Te}}] = 3.03\times 10^{14} T^{\frac{1}{2}} P_{\rm Hg}\exp(-\frac{1.12}{k_BT})$
$\rm Te^{\times}_{I_{Hg}}$	$K_{\rm Te^{\times}_{I_{Hg}}} = [\rm Te^{\times}_{I_{Hg}}] = 7.23\times 10^{29} T^{-\frac{1}{2}} P^{-1}_{\rm Hg}\exp(-\frac{3.38}{k_BT})$
$\rm Te^{\times}_{I_{Te}}$	$K_{\rm Te^{\times}_{I_{Te}}} = [\rm Te^{\times}_{I_{Te}}] = 7.23\times 10^{29} T^{-\frac{1}{2}} P^{-1}_{\rm Hg}\exp(-\frac{3.37}{k_BT})$

The reaction constants for the ionized defects are calculated using Eq. (6) for acceptors and its generalization for donors. We define

$$K_{X^{z\prime}} = [X^{z\prime}] = [X^{\times}]\frac{g_{X^{z\prime}}}{g_{X^{\times}}}\exp(z\mu_F - E^1_a - \cdots E^z_a) = K_{X^{\times}}\frac{g_{X^{z\prime}}}{g_{X^{\times}}}\exp(z\mu_F - E^1_a - \cdots E^z_a) \quad (25)$$

and

$$K_{X^{z\bullet}} = [X^{z\bullet}] = K_{X^{\times}}\frac{g_{X^{z\bullet}}}{g_{X^{\times}}}\exp(E^1_d + \cdots + E^z_d - z\mu_F). \quad (26)$$

C. Defect concentrations in $\rm Hg_{0.8}Cd_{0.2}Te$

Gibbs's phase rule tells us that for a system of three components (A, B, and C) and two phases (zinc blende solid and vapor) there are three degrees of freedom. In evaluating the defect concentrations in $\rm Hg_{0.8}Cd_{0.2}Te$ we have chosen the temperature, the mercury pressure $P_{\rm Hg}$, and the alloy composition x as these specified variables; the tellurium and cadmium pressures, the crystal stoichiometry, and the density of the various native point defects are determined by these conditions.

The reaction constants in Table V are evaluated to determine the concentrations of the various native point defects as a function of temperature and pressure. The Fermi energy is determined by requiring charge neutrality. The activation energies for the shallow donor and acceptor states are taken to be zero; the sensitivity of our results to this assumption is discussed further below.

Figure 2(a)–2(c) show the defect concentrations at various equilibration temperatures. Pressure ranges are chosen so as to stay within the stability region of the material.[6] At all temperatures and pressures considered, the dominant defect is found to be the doubly ionized mercury vacancy, in agreement with previous interpretations of experiments;[1] our result confirms the generally accepted experimental observation that the mercury vacancy is responsible for the p-type behavior of undoped HgCdTe equilibrated at high temperatures.

At all temperatures, the second most dominant defect is found to be the tellurium antisite. The antisite concentration decreases more rapidly with $P_{\rm Hg}$ than does the mercury vacancy, and thus is most important at low mercury pressures. As does the mercury vacancy, the tellurium antisite defect accommodates excess tellurium in the lattice, and therefore its presence also shifts the stoichiometry towards the tellurium-rich side of the phase diagram.

The reason the tellurium antisite concentrations is so high deserves comment. The tellurium antisite formation energy is larger than that for the mercury vacancy by 1 eV (Table III). However, as can be seen from Table V, the pre-exponential factor of the reaction constant for the tellurium antisite is enormous. The large pre-exponential factor results from the large phase space factor (entropy) gained by creating two free mercury atoms compared to that lost by elimination of a formula unit. In contrast, the mercury antisite density is low, despite the fact that

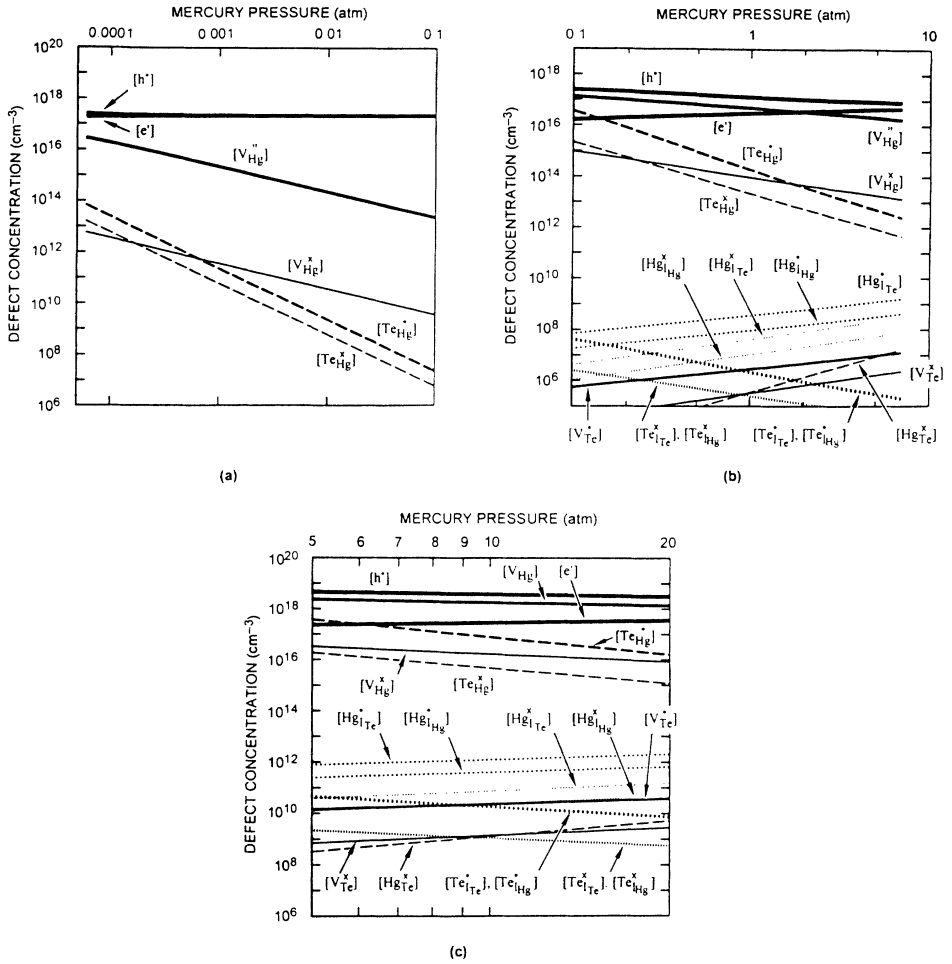

FIG. 2. Defect concentrations at annealing temperature for material annealed at (a) 250°C, (b) 500 °C, and (c) 655 °C.

its formation energy is quite small; this again is a result of the pre-exponential factor that in this case is very small. Thus it is clear that one must be cautious in deducing the relative populations of the various defects based on the electronic contributions to the defect formation energies alone.

While the tellurium antisite is never found to be the dominant defect controlling the doping under equilibrium conditions, it can introduce significant compensation at low mercury pressures. Moreover, the diffusion coefficient of the antisite is expected to be quite small because the diffusion of an antisite will necessarily involve at least one additional point defect, such as the mercury vacancy or the tellurium interstitial. Thus the tellurium antisite may not reach equilibrium densities for the times and temperatures corresponding to the low-temperature (~250 °C), high-mercury-pressure anneals typically employed to reduce the mercury vacancy density. If tellurium antisite densities are in fact equilibrated at a temperature at which the antisite diffusion effectively stops during cool down from the growth temperature, then the antisites may be frozen in at higher, nonequilibrium concentrations. If such a freezing in of nonequilibrium antisites does occur, the tellurium antisite may in fact be the "universal" residual donor observed in densities of $\sim 10^{14}$ cm^{-3} in material subjected to a low-mercury-pressure, high-temperature anneal, although it is not clear why, for example, the frozen-in density of antisites would be the same for LPE material grown from both mercury- and tellurium-rich melts. The tellurium antisite may also be the defect responsible for the n-type carrier concentrations in as-grown MBE material,[8] which is believed to be grown on the tellurium-rich side of the phase diagram where antisite populations are highest.

Annealing strategies for reduction of the tellurium antisite densities can be developed and may be important if the antisite is the residual donor. Consider, for example, a two-temperature annealing process in which a first anneal is done under mercury-saturated conditions, but at the lowest temperature for which the antisite is able to equilibrate in reasonable times. This anneal would serve to lower the antisite densities as much as possible. A second anneal would be much like that currently employed, that is, at ~250 °C under mercury-saturated conditions and would serve to anneal out the mercury vacancies, leaving the antisite densities effectively unchanged.

At 500 °C mercury interstitials are present at levels $\simeq 10^{10}$ cm^{-3} and at no temperatures are present at levels high enough to significantly compensate the mercury vacancies, much less to turn the material n-type under equilibrium conditions. Unlike the tellurium antisites, the mercury interstitials are relatively fast diffusers,[2] and

thus it is unlikely that nonequilibrium densities of interstitials will be frozen in. The mercury interstitial densities that we predict are in quantitative agreement with those needed to explain the diffusion in $Hg_{1-x}Cd_xTe$ in the process simulator developed by Meléndez and Helms.[39] There is some uncertainty in the quantitative predictions of the mercury interstitial densities reported here because of the neglect of the alloy effects that we expect to be more significant than for the mercury vacancy and tellurium antisite. Although this correction will be largest for the mercury interstitial surrounded by four mercury first neighbors, it should also be significant for the interstitial surrounded by four tellurium first neighbors because of the six cation second-nearest neighbors, which are only slightly more distant than the first neighbors.

The mercury antisite and the tellurium vacancy and interstitial densities are all quite low, never exceeding $\sim 10^8$ cm^{-3} at 500 °C. The corrections to these predicted densities may be sizable because of alloy effects, but such corrections should not significantly impact the densities of the mercury vacancy and tellurium antisite.

Figure 2 shows the defect concentrations at the temperatures at which equilibration takes place; in Fig. 3 we show the defect concentrations for material equilibrated at 500 °C, then quench cooled to 77 K. We have assumed that the total defect concentrations are frozen in during the quench, for example, $[V_{Hg}]^{total} = [V_{Hg}^{\times}]+[V_{Hg}^{\prime}]+[V_{Hg}^{\prime\prime}]$ is constant, but that the electrons and holes are allowed to reach a new equilibrium corresponding to the low temperature. Figure 4 shows the low-temperature hole concentrations for such quench-cooled materials as a function of P_{Hg} and T_{anneal}, compared with the experimental results of Vydyanath.[1] The agreement of our theoretical results with the experiments is remarkably good considering that our calculated results are obtained al-

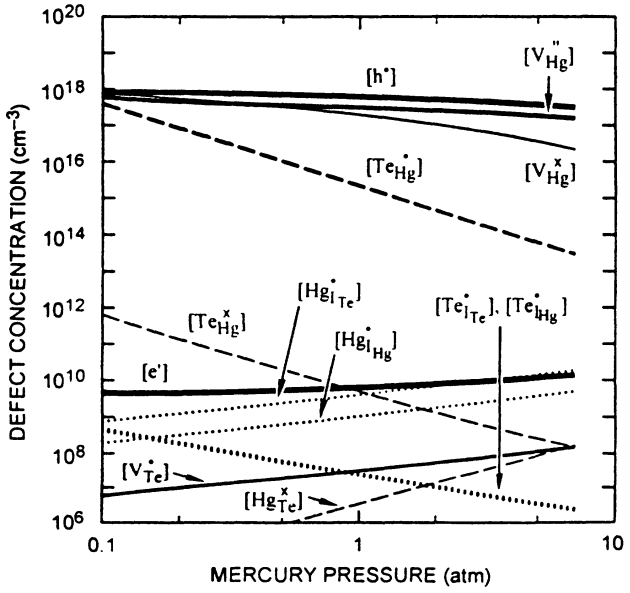

FIG. 3. Defect concentrations for the 500 °C anneal after quench cooling to 77 K.

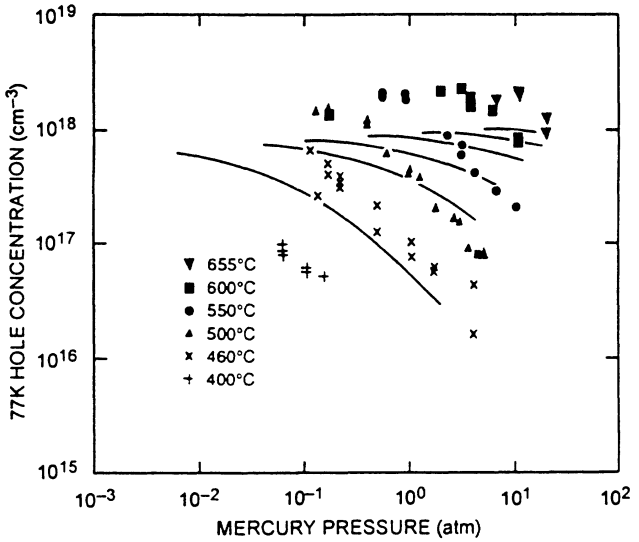

FIG. 4. Hole concentrations at 77 K for material equilibrated at various high-temperature annealing conditions. Experimental results taken from Ref. 1.

most entirely from first principles. Moreover, there is a significant uncertainty in the quenching efficiency of the experiments; thus exact agreement with the experiments is not a valid criterion for testing the accuracy of the theory.

From Fig. 4 one can see that for the higher annealing temperatures our calculations predict a different dependence of hole concentration on the mercury pressure than is experimentally observed. The lower slopes for the theory result from our finding that the material is extrinsic at the higher temperatures. If the material is intrinsic when equilibrated as the experiments indicate, then $[V_{Hg}^{\prime\prime}]_{ht} \propto P_{Hg}^{-1}$, as can be obtained from Table V, with μ_F independent of $[V_{Hg}]$. However, if the material is extrinsic when equilibrated, that is, with $[h^{\bullet}] = 2[V_{Hg}^{\prime\prime}]$, then from the reaction

$$Hg \rightarrow V_{Hg}^{\prime\prime} + 2h^{\bullet} + Hg_{vapor} \tag{27}$$

we see that $[V_{Hg}^{\prime\prime}][h^{\bullet}]^2 \propto [V_{Hg}^{\prime\prime}]^3 \propto P_{Hg}^{-1}$.

The discrepancies between theory and experiments may be due to a number of factors. First, both uncertainty in the quenching efficiencies and analysis of the Hall data may account for some of the discrepancy. There are also a number of uncertainties in the theoretical calculation that may account for the discrepancies. These include uncertainties in the electronic and vibrational defect formation free energy, the ionization energies of the defects (which were assumed to be zero in the above calculations), alloy effects, and finally the uncertainties in the intrinsic reaction constant. These are discussed in turn below.

First it is interesting to examine the sensitivity of our predictions to the accuracy of electronic and vibrational defect formation free energy. In Fig. 5 we have recalculated the 77 K hole concentrations as a function of the annealing temperature with the electronic contribution

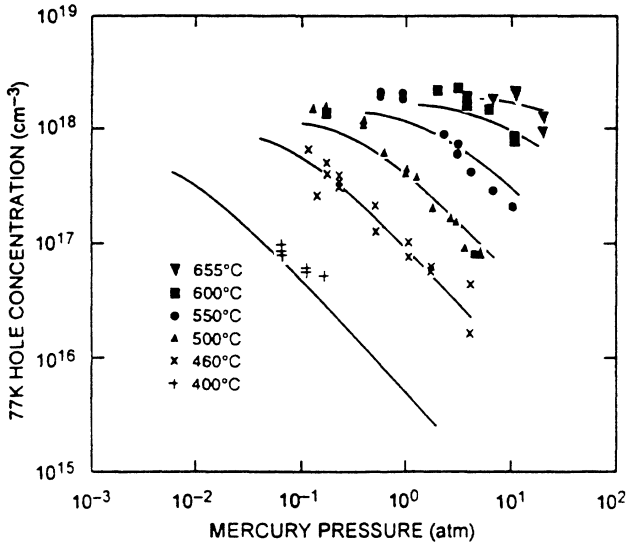

FIG. 5. Hole concentrations at 77 K for material equilibrated at various high-temperature annealing conditions, calculated with the electronic formation energy for the mercury vacancy increased by 10% and a rigid upward shift of the hole concentrations by a factor of 2.2. This figure is meant to demonstrate the sensitivity of our results to small changes in our calculated parameters. As discussed in the text, similar qualitative changes in our results can be seen by modifying the intrinsic reaction constant.

to the mercury vacancy formation energy increased by 10% and a rigid shift upward in our results by a factor of 2.5; such small changes result in better agreement with experiments. The corrections to our calculated mercury vacancy and tellurium antisite formation energies due to alloy effects have not yet been included in these calculations and are expected to be in the range of tenths of an eV, as discussed in Sec. II C, and thus may account for the magnitude of correction used in this example. Preliminary estimates for the corrections for going from the 16-atom to the 32-atom supercell are ~0.1 eV for the cation vacancy and the tellurium antisite as well. Finally, Jahn-Teller relaxation energies have not been included in the present work and they may modify the electronic formation free energies. An increase in the effective vibrational frequencies [$\bar{\omega}$ in Eq. (A20)] can account for an upward shift in the densities. Such an increase may arise from differences between the neutral and ionized defect vibrational free energies and, perhaps, anharmonic effects that may be large at defects such as the vacancy where an atom is missing from the lattice. Thus we see that our calculations agree with the experimental data approximately to within the known uncertainties of the theory.

Our results are also very sensitive to the intrinsic reaction constant, which in turn depends sensitively on the band structure and its temperature dependence. HgCdTe is known to be anomalous in that its band gap is found to increase with temperature at room temperature and below, and although there is no experimental information on the temperature dependence of the gap at higher temperatures, we have assumed that Eq. (21) extrapolates to higher temperatures. In addition, as discussed above, we have assumed a parabolic valence band, but a linear variation of the conduction band, with the slope chosen to agree with the intrinsic carrier concentrations [with the energy gap given by Eq. (21) at temperatures below 400 °C]. While this fit is quite good for the temperature range over which it is fit (from 77 K to 400 K), the reliability of K_{pn} at 250 °C and above for which we have presented our defect density predictions is unknown. To demonstrate the sensitivity of our results to the intrinsic reaction constant we have calculated the 77 K temperature hole concentrations with the conduction band density of states increased a factor of 10 and have found, except at the very highest temperatures, that the calculated hole concentrations vary as P_{Hg}^{-1}, indicating intrinsic behavior at the annealing temperature and resulting in better agreement with experiments. Because our results depend sensitively on the intrinsic reaction constant, it is essential to establish a reliable prediction of its value at the annealing and growth temperatures where equilibration of the defect densities takes place.[35]

We have suggested that nonequilibrium densities of tellurium antisites may be the residual donor, but they may also be important SRH recombination centers. It is experimentally observed that the residual donor does not freeze out even for samples cooled to 4 K, and therefore its first ionization state must resonate in the conduction band. A SRH recombination center in $Hg_{1-x}Cd_xTe$ with $x = 0.22$ lies ~25 meV below the conduction band edge, has a larger capture cross section for electrons than holes, and typically has a density smaller than, but comparable to, the residual donor density. The properties of the antisite are consistent with such a level: it is a donor; although we have assumed here it is a single donor, it is likely that a second donor level is present in the gap and may be ionized at the high processing temperatures; and the first ionization level may be resonant in the conduction band, although we are unable to resolve this in our present calculations with certainty. A more quantitative prediction of the ionization levels of the antisite is needed to correlate it with a SRH center.

A technologically important step in making ir detectors from $Hg_{1-x}Cd_xTe$ is a low-temperature mercury-saturated anneal that is done to reduce the mercury vacancy concentrations. In Fig. 6 we show the defect concentrations for material annealed at various temperatures along the mercury-saturated side of the phase diagram. In such mercury-saturated anneals, if equilibrium can truely be reached, then the mercury vacancies will certainly be the dominant defect, with the tellurium antisite density being negligible. However, as discussed above, it is unlikely that equilibrium densities of antisites will be achieved at these relatively low temperatures.

The above analysis of defect concentrations can be repeated for a number of different situations. For example, we can calculate the native defect densities with a donor or acceptor impurity present. At the high growth temperatures, the impurity concentrations would have to be comparable to the vacancy concentrations to modify the high-temperature vacancy concentration. We can also re-

peat the above calculations for reference state other than the mercury vapor. For example, in HgCdTe tellurium precipitates are known to form as a metastable state upon cooling from high growth temperatures.[40] In the vicinity of a precipitate, the native defect populations will be in local equilibrium with the tellurium solid and defect concentrations for this reference state can be calculated. Because this constitutes a nonequilibrium situation, on must address diffusion rates to assess the extent of the modified defect atmosphere about a precipitate.

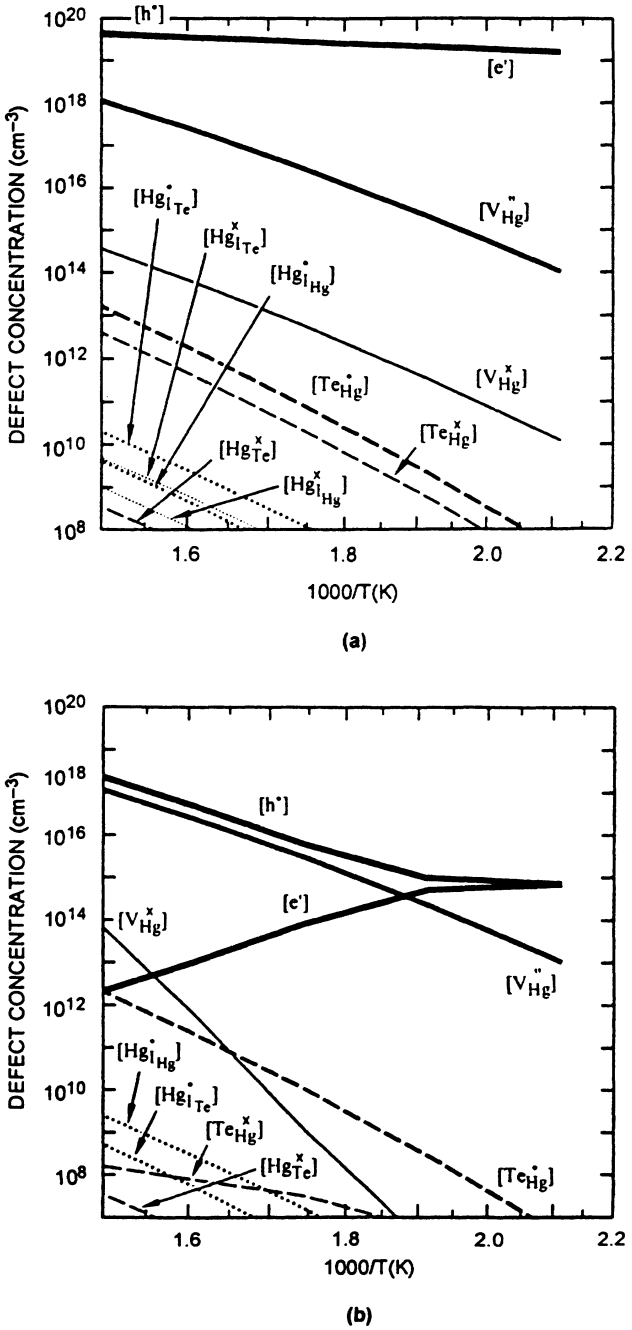

FIG. 6. Defect concentrations for material annealed along the mercury-rich side of the stability region at (a) the annealing temperature and (b) after quenching to 77 K.

VI. SUMMARY AND CONCLUSIONS

We have made quantitative predictions of the native point defect densities in $Hg_{0.8}Cd_{0.2}Te$ as a function of temperature and pressure and find good agreement with the available experiments. We have substantiated the claim that the primary defect is the mercury vacancy and have identified the tellurium antisite as an important secondary defect. A first-principles approach was used for most of the quantities calculated, with the only significant empirical data being those needed to obtain the temperature-dependent intrinsic reaction constant.

Although we predict the undoped material to be always p type, refinements in our calculations may show that the antisite may dominate in the low-mercury-pressure region and turn the material n type by a native defect; our current accuracy is not sufficient to establish this. While most anneals of technological importance are done under mercury-saturated conditions to reduce mercury vacancy concentrations, exploration of the tellurium-saturated region where we predict the tellurium antisite densities become comparable to those of those of the mercury vacancy may help confirm the presence of tellurium antisites.

A second means to explore the presence of tellurium antisites and their relationship to the residual donor is through a careful set of experiments using two temperature anneals, as discussed above. Because we do not know the temperature at which diffusion of tellurium effectively stops, the temperature of the first anneal would have to be varied, as would the annealing time; the mercury pressure could also be varied, although mercury-saturated conditions are those one would eventually want to employ. The identification of the tellurium antisite as the residual donor can be made if the donor densities in identically grown material were found to differ after the second anneal (using the standard conditions for a mercury-saturated low-temperature anneal) depending on the conditions of the first anneal. A quantitative analysis of this experiment would be quite difficult because, in addition to uncertainties in the temperature at which the tellurium antisite equilibration stops, if the tellurium antisite diffuses via a vacancy mechanism, the diffusion of the antisite will depend on the concentration of mercury vacancies present during the first anneal.

It would also be useful to perform high-temperature annealing as was done by Vydyanath,[1] but instead of quenching to 77 K and having to address the issue of quenching efficiency, follow the anneals by Hall analysis at the anneal temperature. Recently, an attempt at such an experiment was made by Wienecke *et al.*,[35] although an analysis of such an experiment requires knowledge of the high-temperature intrinsic reaction constant.

ACKNOWLEDGMENTS

We wish to acknowledge the work of Michael Methfessel in development of the first-principles codes applied in this work. This work has been supported by NASA Contract No. NAS1-18226, ARPA Contract No. MDA972-

92-C-0053, and ONR Contract No. N00014-89-K-132. Computational support was provided by the Numerical Aerodynamical Simulation computing facility at NASA Ames Research Center.

APPENDIX: VIBRATIONAL ENTROPY OF POINT DEFECTS IN SEMICONDUCTORS

As discussed by Keating,[36] we assume the elastic energy for a zinc blende structure can be written as

$$V = \frac{3\alpha}{8d_0^2}\sum_i [\Delta(\vec{r}_i\vec{r}_i)]^2 + \frac{3\beta}{8d_0^2}\sum_{i>i'}[\Delta(\vec{r}_i\vec{r}_{i'})]^2, \quad \text{(A1)}$$

where i and i' sum over all bonds, $\Delta(\vec{r}_i\vec{r}_{i'}) = \vec{r}_i\vec{r}_{i'} - \vec{r}_i^0\vec{r}_{i'}^0$, with $\vec{r}$ and $\vec{r}^0$ the bond vectors connecting adjacent atoms in the distorted and equilibrium lattices, respectively. For first-neighbor interactions, the sum in the second term runs over only those bonds connected to a common atom.

For a nonionic material, the normal modes for the displacement of the atoms are determined by solving the equation of motion for the lattice cast in the usual manner in terms of the three-dimensional eigenvalue equation

$$\omega^2\vec{u} = \mathbf{D}^e(\mathbf{k})\vec{u}. \quad \text{(A2)}$$

Here $\mathbf{D}^e(\mathbf{k})$ is the (elastic) dynamical matrix and

$$\vec{u} = \begin{pmatrix}\vec{u}_1\\ \vec{u}_2\end{pmatrix} \quad \text{(A3)}$$

is the polarization vector of the normal modes, where $\vec{u}_i$ is the displacement vector of the ith atom. For the zinc blende lattice there are two atoms per unit cell, so $i = 1$ or 2.

In terms of the elastic constants, C_{11} and C_{12}, the dynamical matrix for the valence force field model is given by

$$\mathbf{D}^e(\vec{k}) = \begin{pmatrix} \frac{8dC_{11}}{\sqrt{3}m_1}\mathbf{I} & \frac{2dC_{12}}{\sqrt{3m_1m_2}}\mathbf{S}(\vec{k}) + \frac{2d(C_{11}-C_{12})s(\vec{k})}{\sqrt{3m_1m_2}}\mathbf{I} \\ \frac{2dC_{12}}{\sqrt{3m_1m_2}}\mathbf{S}^*(\vec{k}) + \frac{2d(C_{11}-C_{12})s^*(\vec{k})}{\sqrt{3m_1m_2}}\mathbf{I} & \frac{8dC_{11}}{\sqrt{3}m_2}\mathbf{I}\end{pmatrix}, \quad \text{(A4)}$$

where d is the equilibrium bond length, m_1 and m_2 are the masses of the two atoms in the unit cell, $\mathbf{I}$ is the 3×3 unit matrix, and $\mathbf{S}$ is given by

$$\mathbf{S} = \begin{pmatrix} s_1 & s_4 & s_3\\ s_4 & s_1 & s_2\\ s_3 & s_2 & s_1\end{pmatrix} \quad \text{(A5)}$$

with

$$s_1(\vec{k}) = e^{i\vec{k}\cdot\vec{d}_1} + e^{i\vec{k}\cdot\vec{d}_2} + e^{i\vec{k}\cdot\vec{d}_3} + e^{i\vec{k}\cdot\vec{d}_4}, \quad \text{(A6a)}$$

$$s_2(\vec{k}) = e^{i\vec{k}\cdot\vec{d}_1} + e^{i\vec{k}\cdot\vec{d}_2} - e^{i\vec{k}\cdot\vec{d}_3} - e^{i\vec{k}\cdot\vec{d}_4}, \quad \text{(A6b)}$$

$$s_3(\vec{k}) = e^{i\vec{k}\cdot\vec{d}_1} - e^{i\vec{k}\cdot\vec{d}_2} + e^{i\vec{k}\cdot\vec{d}_3} - e^{i\vec{k}\cdot\vec{d}_4}, \quad \text{(A6c)}$$

and

$$s_4(\vec{k}) = e^{i\vec{k}\cdot\vec{d}_1} - e^{i\vec{k}\cdot\vec{d}_2} - e^{i\vec{k}\cdot\vec{d}_3} + e^{i\vec{k}\cdot\vec{d}_4}. \quad \text{(A6d)}$$

The $\vec{d}_j$ are the vectors connecting atom 1 to atom 2 in the unit cell and are given by $d_1 = \frac{a}{4}[111]$, $d_2 = \frac{a}{4}[1\bar{1}\bar{1}]$, $d_3 = \frac{a}{4}[\bar{1}1\bar{1}]$, and $d_4 = \frac{a}{4}[\bar{1}\bar{1}1]$, where a is the lattice constant.

While short-range elastic forces are described within the valence force field model, in crystal with an ionic contribution to the bonding, Coulomb interaction must also be included in the dynamical matrix. The long-range nature of the Coulomb interaction complicates the problem considerably. Using a pairwise point-charge model of the Coulomb interaction, the Coulomb dynamical matrix is given by[37]

$$D^c_{\alpha\alpha'}(\kappa,\kappa'|\vec{k}) = -\frac{\delta_{\kappa,\kappa'}}{m_\kappa}\sum_{\kappa''}\phi_{\alpha\alpha'}(\kappa\kappa''|0) + \frac{1}{\sqrt{m_\kappa m_{\kappa'}}}\phi_{\alpha\alpha'}(\kappa\kappa'|\vec{k}), \quad \text{(A7)}$$

where

$$\phi_{\alpha\alpha'}(\kappa,\kappa'|\vec{k}) = -\frac{q_\kappa q_{\kappa'}}{4\pi\epsilon_0}P^{3/2}\times\sum_{l'}H_{\alpha\alpha'}\{\sqrt{P}[\vec{x}(l,\kappa)-\vec{x}(l',\kappa')]\}e^{i\vec{k}\cdot[\vec{x}(l,\kappa)-\vec{x}(l',\kappa')]} + \frac{q_\kappa q_{\kappa'}}{v_0\epsilon_0}\sum_{\vec{G}}\frac{(\vec{G}+\vec{k})_\alpha(\vec{G}+\vec{k})_{\alpha'}}{|\vec{G}+\vec{k}|^2}\exp\left(\frac{-|\vec{G}+\vec{k}|^2}{4P}\right)\exp\{i\vec{G}[\vec{x}(\kappa)-\vec{x}(\kappa')]\}. \quad \text{(A8)}$$

In the above equation l and κ label the unit cell and basis atoms, α refers to the Cartesian component, q_κ is the effective charge, $\vec{x}(\kappa,l) = \vec{x}(\kappa) + \vec{x}(l)$ is the position vector of the κth atom in the lth unit cell, $\vec{G}$ are the reciprocal lattice vectors, v_0 is the unit cell volume, ϵ_0 is the permitivity constant, and P is a (numerically determined) measure of the Gaussian charge distribution used in the Ewald summation. $H_{\alpha,\alpha'}(y)$ is given by the

integro-differential expression

$$H_{\alpha,\alpha'}(y) = \frac{2}{\sqrt{\pi}} \frac{\partial}{\partial y_\alpha} \frac{\partial}{\partial y_\beta} \left(\frac{1}{y} \int_y^\infty \exp(-x^2) dx \right). \quad \text{(A9)}$$

The full dynamical matrix is given by the sum of the Coulomb and elastic contributions

$$\mathbf{D}(\vec{k}) = \mathbf{D}^c(\vec{k}) + \mathbf{D}^e(\vec{k}). \quad \text{(A10)}$$

In the present problem we are interested in calculating the change in the vibrational free energy of the crystal lattice due to the creation of a defect. This is done using the Green's function, which is most conveniently calculated in terms of the density of states of the phonon system. For the ideal crystal without a defect, a Brillouin zone integration is done to calculate the phonon density-of-states matrix $\mathbf{\Theta}$, from which the Green's function can be calculated via

$$\mathbf{G}^0(\omega^2) = \int_{\omega^2_{\min}}^{\omega^2_{\max}} \frac{\mathbf{\Theta}(\omega'^2) - \mathbf{\Theta}(\omega^2)}{\omega'^2 - \omega^2 - i\eta} d\omega'^2 + \mathbf{\Theta}(\omega^2) \ln\left(\frac{\omega^2 - \omega^2_{\min} - i\eta}{\omega^2 - \omega^2_{\max} - i\eta} \right), \quad \text{(A11)}$$

where the singularity in the integral has been explicitly removed. The change in the total density of states when a defect is introduced into the crystal can be deduced from Dyson's equation to obtain

$$\Delta\mathbf{\Theta}(\omega^2) = \frac{1}{\pi} \mathrm{Im} \frac{\partial}{\partial \omega^2} \ln\{\det[1 - \mathbf{G}^0(\omega^2)\mathbf{V}]\}, \quad \text{(A12)}$$

where $\mathbf{V}$ is the perturbation potential. In the present case we use a strictly site-diagonal perturbation potential corresponding to the mass change due to the introduction of an isolated defect.

The partition function for the phonon system in the zinc blende lattice is given by

$$Z = \prod_i \left(\frac{\exp\left(\frac{-\hbar\omega_i}{2k_BT}\right)}{1 - \exp\left(\frac{-\hbar\omega_i}{k_BT}\right)} \right), \quad \text{(A13)}$$

where ω_i are the normal modes of the system. The total vibrational entropy of the system is obtained from $S^{\mathrm{vib}}_{\mathrm{total}} = \frac{\partial}{\partial T}(k_BT \ln Z)$, which gives

$$S^{\mathrm{vib}}_{\mathrm{total}} = \sum_i \left\{ k_B \ln\left[\frac{1}{2} \sinh^{-1}\left(\frac{\hbar\omega_i}{2k_BT} \right) \right] + \frac{\hbar\omega_i}{2T} \coth\left(\frac{\hbar\omega_i}{2k_BT} \right) \right\}. \quad \text{(A14)}$$

We convert the sum to an integral by the replacement

$$\sum_i \to \int_0^\infty \rho(\omega) d\omega = \int_0^\infty 2\rho(\omega^2)\omega d\omega \quad \text{(A15)}$$

where $\rho(\omega^2) = \mathrm{Tr}\mathbf{\Theta}(\omega^2)$. We are interested in the change in the vibrational entropy upon formation of a defect, in which case we replace ρ by $\Delta\rho$ to obtain

$$S^{\mathrm{vib}} = 2k_B \int_0^\infty \Delta\rho(\omega^2) \left\{ \frac{\hbar\omega}{2k_BT} \coth\left(\frac{\hbar\omega}{k_BT} \right) - \ln\left[2\sinh\left(\frac{\hbar\omega}{2k_BT} \right) \right] \right\} \omega d\omega. \quad \text{(A16)}$$

Similarly for the vibrational energy, we use the relationship $U^{\mathrm{vib}} = -\frac{\partial}{\partial(1/k_BT)} \ln Z$ to obtain

$$U^{\mathrm{vib}} = 2 \int_0^\infty \Delta\rho(\omega^2) \left[\frac{\hbar\omega}{2} \coth\left(\frac{\hbar\omega^2}{2k_BT} \right) \right] \omega d\omega, \quad \text{(A17)}$$

with the change in the vibrational free energy $F^{\mathrm{vib}} = U^{\mathrm{vib}} - TS^{\mathrm{vib}}$.

While the calculation of the vibrational terms in this paper was done using the general expressions above, it is interesting to examine the expression for the free energy in the high-temperature limit, which is appropriate for high growth and processing temperatures, and to examine the explicit temperature dependence of this term. In the high-temperature limit $\hbar\omega_{\max} \ll k_BT$ and F^{vib} reduces to

$$F^{\mathrm{vib}} \approx 2k_BT \int_0^\infty \ln\left(\frac{\hbar\omega}{k_BT} \right) \rho(\omega)\omega d\omega. \quad \text{(A18)}$$

This integral can be shown to be equal to

$$F^{\mathrm{vib}} \approx k_BT n_m \ln\left(\frac{\hbar\bar{\omega}}{k_BT} \right), \quad \text{(A19)}$$

where n_m is the number of phonon modes created or destroyed in the defect reaction of interest and $\bar{\omega}$ is an appropriately weighted frequency. What enters the calculation of the defect concentrations is $\exp(-F^{\mathrm{vib}}/k_BT)$, which reduces to

$$\exp\left(\frac{F^{\mathrm{vib}}}{k_BT} \right) \approx \left(\frac{k_BT}{\hbar\bar{\omega}} \right)^{n_m} = CT^{n_m} \quad \text{(A20)}$$

in the high-temperature limit. For the defect reactions in Table I we obtain

$$n_m = \begin{cases} -3 & V_{\mathrm{Hg}} \\ 3 & V_{\mathrm{Te}} \\ 6 & \mathrm{Hg}_{\mathrm{Te}} \\ -6 & \mathrm{Te}_{\mathrm{Hg}} \\ +3 & \mathrm{Hg}_I \\ -3 & \mathrm{Te}_I \,. \end{cases} \quad \text{(A21)}$$

We will use this simple power-law dependence of Eq. (A20) to extract a simple power-law temperature dependence of the reaction constants.

[1] H. R. Vydyanath, J. Electrochem. Soc. **128**, 2609 (1981).
[2] D. A. Stevenson and M-F. S. Tang, J. Vac. Sci. Technol. B **9**, 1615 (1991), and references therein.
[3] S. M. Johnson, D. R. Rhiger, J. P. Rosbeck, J. M. Peterson, S. M. Taylor, and M. E. Boyd, J. Vac. Sci. Technol. B **10**, 1499 (1992).
[4] S. H. Shin, J. M. Arias, D. D. Edwall, M. Sandian, J. G. Pasko, and R. E. DeWames, J. Vac. Sci. Technol. B **10**, 1492 (1992).
[5] R. S. List, J. Electron. Mater. **22**, 1017 (1993).
[6] H. R. Vydyanath, J. Appl. Phys **65**, 3080 (1989).
[7] M. C. Chen, S. G. Parker, and D. F. Weirauch, J. Appl. Phys. **58**, 3150 (1985).
[8] R. Sporken, M. D. Lange, S. Sivanathan, and J. P. Faurie, Appl. Phys. Lett. **59**, 81 (1991).
[9] G. A. Baraff and M. Schlüter, Phys. Rev. Lett. **55**, 1327 (1985); Phys. Rev. B **30**, 1853 (1984); G. A. Baraff, E. O. Kane, and M. Schlüter, *ibid.* **21**, 5662 (1980).
[10] D. B. Laks, C. G. Van de Walle, G. F. Neumark, and S. T. Pantelides, Phys. Rev. Lett. **66**, 648 (1991); D. B. Laks, C.G. Van de Walle, G. F. Neumark, P.E. Blöchl, and S. T. Pantelides, Phys. Rev. B **45**, 10 965 (1992).
[11] J. Bernholc N. O. Lipari, and S. T. Pantelides, Phys. Rev. B **21**, 3545 (1980); J. Bernholc and S. T. Pantelides, *ibid.* **18**, 1780 (1978); J. Bernholc, N. O. Lipari, and S. T. Pantelides, Phys. Rev. Lett. **41**, 895 (1978).
[12] S. B. Zhang and D. J. Chadi, Phys. Rev. Lett. **64**, 1789 (1990).
[13] M. A. Berding, M. van Schilfgaarde, A. T. Paxton, and A. Sher, J. Vac. Sci. Technol. A **8**, 1103 (1990).
[14] M. A. Berding, M. van Schilfgaarde, and A. Sher, J. Vac. Sci. Technol. B **10**, 1471 (1992).
[15] M. A. Berding, A. Sher, and A.-B. Chen, J. Appl. Phys. **68**, 5064 (1990); J. Vac. Sci. Technol. A **5**, 3009 (1987).
[16] J. T. Schick and C. G. Morgan-Pond, J. Vac. Sci. Technol. A **8**, 1108 (1990); C. G. Morgan-Pond and R. Raghavan, Phys. Rev. B **31**, 6616 (1985).
[17] M. A. Berding, M. van Schilfgaarde, and A. Sher, J. Electron. Mater. **22**, 1005 (1993).
[18] O. K. Andersen, O. Jepsen, and D. Glotzel, *Highlights of Condensed Matter Theory*, edited by F. Bassani *et al.* (North-Holland, Amsterdam, 1985), p. 59.
[19] D. Langreth and D. Mehl, Phys. Rev. B **28**, 1809 (1983).
[20] M. van Schilfgaarde, A.T. Paxton, M. A. Berding, and M. Methfessel (unpublished).
[21] F. A. Kröger, *The Chemistry of Imperfect Crystals* (J. Wiley & Sons, Inc., New York, 1964).
[22] F. A. Kröger and H. J. Vink, in *Solid State Physics Vol. 3*, edited by F. Seitz and D. Turnbull (Academic Press, New York, 1956), p. 307.
[23] S. Krishnamurthy and A. Sher (unpublished).
[24] M. Methfessel and M van Schilfgaarde (unpublished).
[25] U. von Barth and L. Hedin, J. Phys. C **5**, 1629 (1972).
[26] M. Methfessel, Phys. Rev. B **38**, 1537 (1988).
[27] R. Jones and A. Sayyesh, J. Phys. C **19**, L653 (1986).
[28] J. P. Hirth and J. Lothe, *Theory of Dislocations* (J. Wiley & Sons, Inc., New York, 1982), p. 49.
[29] E. R. Weber, H. Ennen, U. Kaufmann, J. Windscheif, J. Schneider, and T. Wosinski, J. Appl. Phys. **53**, 6140 (1982).
[30] C. G. Van de Walle, P. J. H. Denteneer, Y. Bar-Yam, and S. T. Pantelides, Phys. Rev. B **39**, 10791 (1989).
[31] D. E. Cooper and W. A. Harrison, J. Vac. Sci. Technol. A **8**, 1112 (1990).
[32] For a general discussion of the calculation of state degeneracy in semiconductors, see E. A. Guggenheim, Proc. Phys. Soc. London Sect. A **66**, 121 (1953), and references therein.
[33] G. L. Hansen and J. L. Schmit, J. Appl. Phys. **54**, 1639 (1983).
[34] G. L. Hansen, J. L. Schmit, and T. N. Casselman, J. Appl. Phys. **53** 7099, (1982).
[35] There has been a recent attempt to predict the intrinsic carrier concentrations at temperatures up to 600 °C by M. Wienecke, M. Schenk, and H. Berger, Semicond. Sci. Technol. **8**, 299 (1993), although their analysis is suspect because of the temperature dependences they have assumed for the high-temperature mobility.
[36] P. N. Keating, Phys. Rev. **145**, 637 (1966).
[37] A. A. Maradudin, E. W. Montroll, G. H. Weiss, and I. P. Ipatova, in *Solid State Physics*, edited by H. Ehrenreich, F. Seitz, and D. Turnbull (Academic Press, New York, 1971), Suppl. 3, p. 1.
[38] W. A. Harrison, *Electronic Structure and the Properties of Solids* (W. H. Freeman and Company, San Francisco, 1980).
[39] J. L. Meléndez and C. R. Helms (unpublished).
[40] H. F. Schaake and J. H. Tregilgas, J. Electron. Mater. **12**, 931 (1983).